Reduction of Oxygen Vacancy Related Traps in TiO_2 and the Impacts on Hybrid Perovskite Solar Cells

Yu-Che Ho[1†], Md Nadim Ferdous Hoque[1†], Elizabeth Stoneham[1], Juliusz Warzywoda[2], Tim Dallas[3], Zhaoyang Fan[1*]

[1]Department of Electrical and Computer Engineering and Nano Tech Center, Texas Tech University, Lubbock, TX 79409, USA

[2]Materials Characterization Center, Whitacre College of Engineering, Texas Tech University, Lubbock, TX 79409, USA

[3]Department of Electrical and Computer Engineering, Texas Tech University, Lubbock, TX 79409, USA

(* Contact author: Zhaoyang.Fan@ttu.edu)

([†] Y. Ho and M.N.F. Hoque contributed equally)

ABSTRACT

One major problem in the application of TiO_2 and other oxides as an electron transport layer and optical window in perovskite solar cells (PSCs) is the non-stoichiometric defects related to oxygen vacancies. We report the studies of a TiO_2 compact layer annealed in ambient air and in an oxygen environment, and the consequences on planar PSC performance. Chemical analysis and optical studies indicate that oxygen vacancy density can be significantly reduced by changing annealing conditions, leading to higher optical transmission of the TiO_2 layer and retarded carrier recombination in the PSC. The carrier dynamics studies found that the electron recombination lifetime was significantly increased. With an improved electron transport layer, the power conversion efficiency of PSCs with a TiO_2 compact layer annealed in oxygen was increased from 13.58% to 15.85%, due to a largely enhanced current density when comparing to the control PSCs with TiO_2 annealed in ambient air.

INTRODUCTION

With the rapid progress in terms of both power conversion efficiency and fundamental understanding of material and device physics, hybrid organic-inorganic lead halide perovskite solar cells (PSCs) have become one of the most promising next-generation solar cells, considering their potential in both efficiency and cost-effective production.[1-5] In a conventional PSC, the perovskite active layer is sandwiched between the electron transport material (ETM) layer and the hole transport material (HTM) layer to form a double heterojunction structure. In addition to the perovskite active material, ETM and HTM, by selectively accepting one category of photo carriers and reflecting the opposite one, play critical roles in determining the cell power conversion efficiency (PCE), stability and other performances. Study and optimization of these carrier transport materials are therefore essential for maturation of PSC technology.

Several wide bandgap metal oxide materials have been widely used as an effective ETM with superior electron selecting and hole blocking ability, in addition to being employed as a transparent window. Of these oxides, anatase titanium dioxide (TiO_2), an extensively-studied ETM used in dye-sensitized solar cells (DSSC),[4,6] is also the common candidate for PSCs. State-of-the-art PSCs employ either nano-crystalline mesoporous TiO_2 structures or compact TiO_2 layers as an ETM to facilitate electron collection and improve the device stability; this attests to the critical role of TiO_2 in PSCs.[1,7,8] A major challenge in the application of TiO_2 and other oxides is the presence of non-stoichiometric defects related to oxygen vacancies. These defects were found to easily appear during the thermal annealing process.[9,10] When using such oxides as an ETM in DSSCs or PSCs, the oxygen vacancy related defects cause several issues that diminish the cell performance.[11-14] These defects form trap states in the bandgap, and therefore retard the transfer of photo electrons from the active layer to the electrode. In addition, these deep-level states in TiO_2, when located

close to the interface with perovskites, will block the efficient injection of electrons from perovskite to TiO_2 ETM and dramatically enhance the charge recombination at the interface, as recently confirmed both experimentally and theoretically.[15] Therefore, interface engineering can improve the PSC performance.[16] It was further proposed that TiO_2 oxygen vacancy migration in the electric field, which leads to variation of interfacial charge transfer and recombination rates, might also contribute the anomalous hysteresis observed in PSCs.[15]

In the most common approach, the TiO_2 compact layer is deposited in a solution process via spin-coating or screen-printing, followed by thermal annealing in ambient air. A TiO_2 layer produced this way could have a high density of vacancy related defects. The defects in a TiO_2 film is mostly related to the vacancy from Ti^{3+} states which can even vary from bulk to surface across the film thickness.[17] Several methods have been reported to modify a TiO_2 ETM by minimizing oxygen vacancy density or passivating these traps toward improving its charge transport performance. These includes doping with Mg,[18] Nb,[19] Y,[20] Sn,[21] Fe,[22] and F,[23] sputter deposition with reduced oxygen vacancies,[24,25] and morphology modification by using inverse opal formed structure.[26] Also, it has been reported that the oxygen vacancy defects could be decreased by oxygen plasma treatment, as demonstrated in DSSCs[27,28] and PSCs[15] studies. In addition, TiO_2 surface treating and interface engineering by using self-assembled monolayer Fullerene C60, and its derivatives such as PCBM including PC60BM ([6,6]-phenyl-C61-butyric acid methyl ester) or PC70BM ([6,6]-phenyl-C71-butyric acid methylester),[29,30] graphene quantum dots,[31] acetylacetonated-based additives,[32] and many others,[33-35] have been extensively studied. Park *et al.* has summarized these defects related issues and recent progress on the way to eliminate these defects in a recent review article.[36]

Each of these approaches has its pros and cons. When considering low-cost and large-scale

production of PSCs, modification of the thermal annealing process of a TiO_2 layer to minimize the oxygen vacancy density and its adverse consequences, if achievable, shall be a simple and effective approach, and therefore is worthy of investigation.

Herein, we report annealing of solution-processed TiO_2 compact layer in ambient air and oxygen, and its effect on planar PSC performance. It was found that by annealing TiO_2 in oxygen instead of the commonly used ambient air, its oxygen vacancy density can be significantly reduced, which leads to higher optical transmission and slower carrier recombination. X-ray photoelectron spectroscopy (XPS) and cathodoluminescence (CL) investigations confirmed the densities of oxygen vacancy defects can be reduced by changing the annealing conditions. As a consequence, the charge recombination lifetime is significantly extended. The PCE of PSCs with the oxygen annealed TiO_2 compact layer was increased from 13.58% to 15.85%, when comparing to the control PSCs due to a largely enhanced current density.

EXPERIMENTS

Perovskite Solar Cell Fabrication

Prior to the device fabrication, a FTO-coated glass substrate was patterned by etching with Zn metal powder and 2M HCl diluted in deionized water. The patterned substrate was cleaned by successive sonication in detergent, distilled water, acetone, and 2-propanol, each sonication step carried out for 15 min, and then treated with oxygen plasma for 10 min. The precursor of TiO_2 was prepared by dropwise addition of 35 μL of titanium isopropoxide into the mixing solution of 35 μL of 2 M HCl and 4.965 mL of ethanol under stirring. A TiO_2 compact layer was deposited onto the substrate by spin-coating at 2000 rpm for 30 s. Subsequently, the TiO_2 compact layer was sintered in different atmospheres at 500 °C in an oven. For annealing in an oxygen environment,

the oven gas inlet was connected to an oxygen cylinder with steady flow of 10 LPM at 5 PSI injecting pressure, while its outlet is slightly opened to maintain at 1 atm pressure. The oven was purged prior to the oxygen sintering process. For annealing in ambient air, both the inlet and outlet of the oven were opened to the air atmosphere. During annealing, the temperature was ramped up at a rate of 15°C per min until 500ºC was reached, and then was maintained at this temperature for the given duration. After that the oven was cooled down naturally. For the materials characterization study, a TiO_2 compact layer was directly deposited on glass without a FTO contact layer.

The $CH_3NH_3PbI_3$ ($MAPbI_3$) perovskite precursor solution was synthesized by dissolving 646 mg of PbI_2 and 222 mg of methylammonium iodide (MAI) in 900 µL anhydrous N,N-dimethylformamide (DMF) and then adding 100 µL dimethyl sulfoxide (DMSO). The precursor was spin-coated on the prepared substrate through a three-step process using spinning speeds of 500, 3500, and 5000 rpm for 3, 10, and 30 s, respectively. 600 µL of toluene, used as an anti-solvent, was dropped on the spinning substrates at the ninth second. The sample was then annealed on a hot plate at 70 °C for 5 min, and then at 130 °C for 10 min in air in a 30% R.H. hydration chamber. A solid perovskite layer with thickness of ~400 nm and grain size of 1.5 to 2.0 µm was obtained.

75 mg of the hole transport material (HTM), Spiro-OMeTAD, was dissolved in 1 mL chlorobenzene with the addition of 18 µL bis-(trifluoromethyl-sulfonyl)-imide lithium salt (LiTFSI) and 28 µL 4-tert-butylpyridine (TBP). The HTM solution was spin-coated onto the perovskite film at 4500 rpm for 30 seconds. The sample was then kept in a dry box under dark conditions for 3 hours to adequately oxidize the HTM. The device was then fabricated with Au (100 nm) as the back electrode through e-beam evaporation under vacuum.

Solar Cell Characterization

The photovoltaic characteristics were obtained with a SS50 Solar Simulator (Photo Emission Tech, America) under AM 1.5 simulated irradiation (100 mW cm^{-2}). The current density-voltage (J-V) characteristics were recorded by using Keithley 2400 SourceMeter SMU instruments. The scan rate was 10 mV/s with scan delay time 10 ms. The charge carrier dynamics was characterized via open circuit photovoltage decay measurement. The electrochemical impedance spectroscopy (EIS) measurement of PSCs was recorded by using an electrochemical workstation with the frequency range from 1 MHz down to 100 mHz in a nitrogen glove box under zero bias with light illumination.

Materials Characterization

X-ray photoelectron spectroscopy (XPS) measurements were performed on a Physical Electronics PHI 5000 Versa Probe spectrometer using a monochromatic Al Kα (hν = 1486.6 eV) X-ray source. Peaks reported were charge corrected using the adventitious carbon C 1s peak at 284.6 eV as the reference. The room temperature cathodoluminescence (CL) spectra were acquired at 7 kV accelerating voltage with an e-beam current of 100 μA. Transmission spectra of the TiO_2 layer were measured by an UV-Vis-NIR UV-3600 spectrophotometer (Shimadzu, Japan).

RESULTS AND DISCUSSION

The SEM image in Figure 1a shows the typical surface morphology of the hybrid perovskite film deposited on the ~ 45 nm thick TiO_2 compact layer, with a grain size up to ~ 2 μm. There is no discernable morphology change for the perovskite film when the TiO_2 compact layer was annealed under different conditions. Figure 1b is the cross-sectional SEM image of the PSC

structure, indicating the FTO, TiO_2, $MAPbI_3$, and HTM layers. The $MAPbI_3$ perovskite layer has a thickness of ~ 400nm. There are no perovskite grains stacked up on each other in the vertical direction, and therefore large grains will facilitate charge carrier transport and their collection.

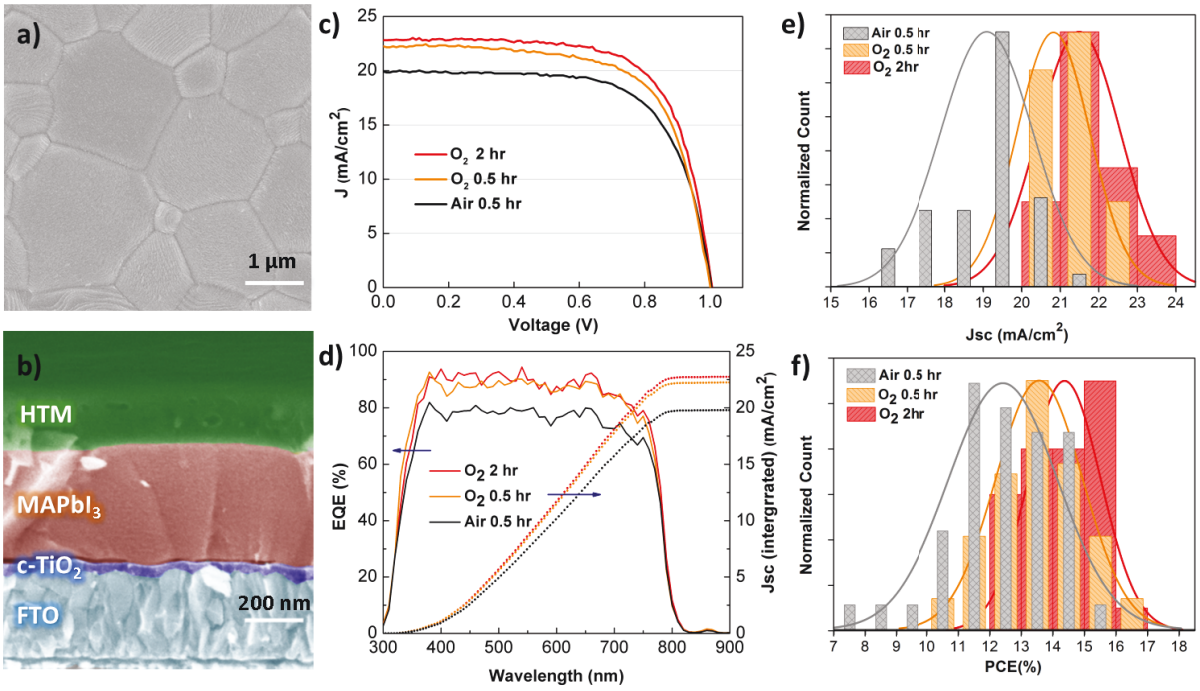

Figure 1. (a) SEM image of perovskite surface morphology showing large crystalline grains. (b) Cross-sectional SEM image of the PSC structure (before Au contact deposition). Pseudo colors were applied to differentiate each layer. (c) Current density-voltage curves for the three different cells based on TiO_2 annealed under different conditions. (d) The corresponding external quantum efficiency and the integrated photocurrent density for the cells in (c). (e) The photocurrent distribution histogram for the three category of cells. (f) The PCE distribution histogram for the three category of cells.

PSCs with TiO_2 ETM annealed in ambient air for 0.5 h, oxygen for 0.5 h, and oxygen for 2 h are called PSC1, PSC2, and PSC3, respectively. The photocurrent-voltage characteristics of these three categories of PSCs are shown in Figure 1c, while the quantum efficiency measurements and

the integrated currents (Figure 1d) were used to calibrate the short circuit current J_{sc}. The *J-V* curves were obtained in the reverse scan from the open voltage to the short circuit at a rate of 10 mV/s. For these champion devices obtained with TiO_2 annealed in different conditions, an increase of J_{sc} from 19.93 mA/cm^2 to 22.26 mA/cm^2 was observed after the annealing atmosphere was changed from ambient air to oxygen while maintaining the 0.5 h annealing duration. J_{sc} was even further increased to 22.82 mA/cm^2 after a longer period (2 h) of oxygen treatment. With a similar open circuit voltage (V_{oc}) but an enhanced fill factor (*FF*), the PCE was thus improved from 13.58% to 15.85%. The photovoltaic parameters of these three champion devices are compared in Table 1.

Table 1. The PSC performance comparison for different TiO_2 annealing conditions.

Sample	J_{sc} (mA/cm^2)	V_{oc} (V)	*FF* (%)	*PCE* (%)	Average J_{sc} (mA/cm^2)	Average *PCE* (%)
PSC1 (Air 0.5 h)	19.93	1.03	66.14	13.58	19.09 ± 1.35	12.41 ±1.95
PSC2 (O_2 0.5 h)	22.26	1.03	65.40	15.00	20.82 ± 1.04	13.57 ± 1.50
PSC3 (O_2 2 h)	22.82	1.03	67.45	15.85	21.52 ± 1.17	14.38 ± 1.25

Considering the PSC performance variation from the same process batch, multiple cells were fabricated and characterized. The J_{sc} and PCE histograms are summed up in Figure 1e,f. It is clear that with the TiO_2 annealing atmosphere changed from air to O_2 and the annealing time changed from 0.5 h to 2 h, the short circuit current and power conversion efficiency of these cells, statistically speaking, were improved. The average J_{sc} was increased from 19.09, 20.82 to 21.52 mA/cm^2, and PSC from 12.41%, 13.57% to 14.38% for the three annealing conditions (Table 1).

In the entire fabrication process of these PSCs, the thermal annealing condition of TiO_2 compact layers was the only parameter that was changed. In order to clarify how annealing condition change of ETM could lead to better photocurrent and power conversion efficiency in PSCs, three TiO_2 samples: annealed in air for 0.5 h (S1), in O_2 for 0.5 h (S2) and in O_2 for 2 h (S3) were studied to understand their property change and the subsequent impact on electron transport in PSCs.

XPS studies were carried out to characterize the variation of oxygen vacancy density in the TiO_2 film surface. The survey spectra of the three samples showed no discernible difference. The high-resolution Ti 2p, O 1s and C 1s core level XPS spectra were then recorded. Detailed analysis of Ti $2p_{2/3}$ component is shown in Figure 2a-c. For each sample, the Ti $2p_{2/3}$ peak was deconvoluted into two symmetric peaks at around 458.8 eV and 457.3 eV. The former peak (458.8 eV) corresponds to $Ti^{4+}{}_{(2p2/3)}$ state, while the latter peak (457.3 eV) could originate either from $Ti^{3+}{}_{(2p2/3)}$ state or from core level peaks of Ti^{4+} bound to an oxygen vacancy (Ti^{4+}–V_O). It was argued that the peak separation between Ti^{4+} and Ti^{3+} is around 1.8–1.9 eV,[37] while the peak separation measured here is around 1.4–1.5 eV, and therefore, the small shoulder (457.3 eV peak) should be attributed to core level peak of Ti^{4+} bound to an oxygen vacancy Ti^{4+}–V_O.[38] Regardless of its origin, oxygen-deficiency during annealing results in this shoulder peak. From our measurements, the area ratio of this shoulder peak to both peaks is reduced from 6.66% in S1 to 6.31% in S2, and further to 3.68% in S3. These differences imply that Ti ions with a lower oxidation state or bounded to an oxygen vacancy as non-stoichiometric defects were oxidized/repaired, and the oxygen deficiency in the film was thus reduced by treatment in the oxygen environment at longer duration. With more stoichiometric structures in the TiO_2 compact layers, the density of the oxygen vacancy defects was reduced.

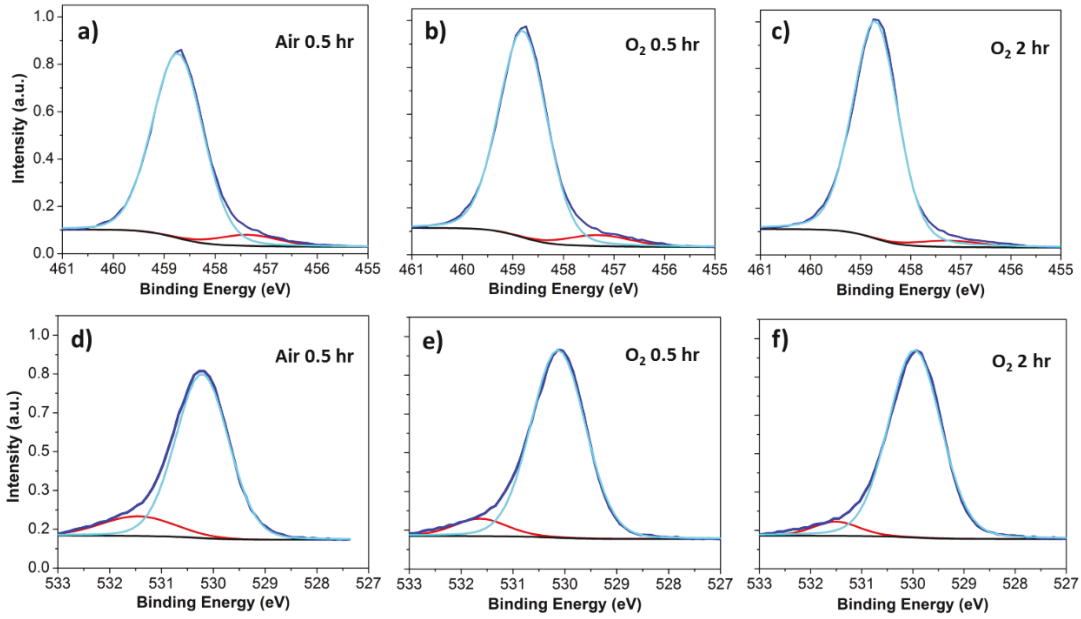

Figure 2. The high-resolution Ti $2p_{3/2}$ peak is deconvoluted into two peaks at around 458.8 eV (main peak) and 457.3 eV (shoulder peak) for three TiO_2 samples: S1 in (a), S2 in (b) and S3 in (c). Similarly, high-resolution O 1s peak is deconvoluted into two peaks at around 530.1 eV (main peak) and 531.5 eV (shoulder peak) for three TiO_2 samples: S1 in (d), S2 in (e) and S3 in (f).

Similar conclusion can also be drawn from the XPS analysis of O 1s peak, which was deconvoluted into a pair of symmetric peaks, as shown in Figure 2d-f. The dominant peak at around 530.1 eV is unambiguously attributed to O–Ti^{4+} bond, while the shoulder peak at around 531.5 eV could be ascribed to O–Ti^{3+} or O–Ti^{4+}– V_O. For the three (S1, S2, and S3) samples, the area ratio of the shoulder peak to both peaks is reduced from 13.81% to 8.76%, and further to 6.32% when annealing in oxygen for 0.5 h and 2 h, respectively. Although the area ratios of the shoulder peak obtained from O 1s spectra are somewhat different when compared to the area ratios obtained from Ti 2p spectra, probably due to surface contamination that introduces other oxygen bonds such as

OH bond, the decreasing trend of the shoulder peaks, and therefore, the conclusion that annealing in oxygen can reduce the oxygen deficiency in a TiO_2 film, is the same.

Since the oxidation of TiO_2 during the annealing process starts from the surface and gradually penetrates into the film "bulk", and because XPS is a surface-sensitive characterization technique, the XPS-measured oxygen deficiency differences determined for the three samples, although exhibiting the changing trend, are not necessarily the most informative/appropriate when considering the entire thickness of TiO_2 film. Low-voltage cathodoluminescence (CL) spectroscopy measurements were carried out to better quantify the effect of oxygen annealing on TiO_2 oxygen vacancies defects in the film "bulk". CL spectroscopy is widely applied as an effective technique for the study of defects in metal oxides,[39,40] and the optical property of a TiO_2 film greatly depends on its stoichiometry.[39,41,42] In our measurements, the overall intensity of the CL spectra significantly increased with the introduction of oxygen annealing. Figure 3 shows the normalized CL spectra of the three (S1-S3) samples annealed in different conditions, and a shoulder peak at longer wavelengths is clearly discernible. At room temperature, band edge transition in TiO_2 is not observable, and the measured spectrum in the visible range comes from sub-band optically active defects and bounded excitons. Based on TiO_2 subband optical transitions, the spectrum was fitted with three Voigt peaks centered at 500, 550, and 610 nm, respectively.[39] Relevant to this study, the red emission at 610 nm was attributed to optically active oxygen vacancy sites.[43,44] For the three samples in Figure 3a-c, the intensity ratio (area ratio) of the 610 nm peak emission to the overall emission decreased from 52.6% to 43.2% and 34.3%, respectively. This suggests that after annealing in oxygen environment, particularly at longer duration, the density of oxygen vacancy sites in the "bulk" film is significantly reduced.

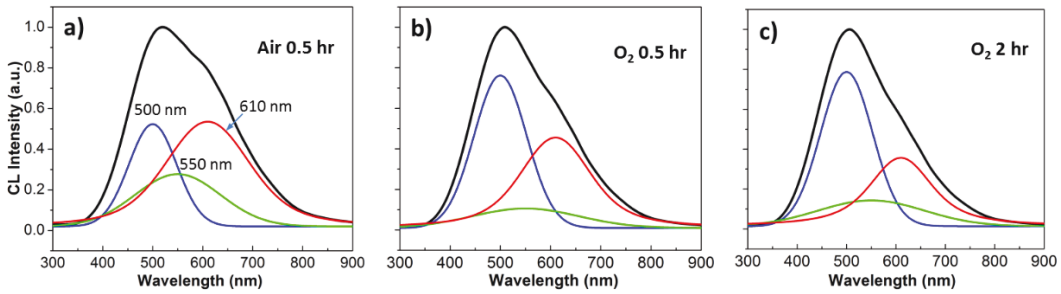

Figure 3. The retrieved CL spectra and their sub-band deconvolution for TiO_2 samples: S1 in (a), S2 in (b), and S3 in (c). All spectra were normalized and fitted with three Voigt functions centered at 500, 550, and 610 nm. The 610 nm red emission is considered to originate from optically active oxygen vacancy sites.

TiO_2 material property change after annealing in oxygen can be further observed from the UV-visible transmission spectra, as shown in Figure 4. The optical transmission at wavelengths below ~ 500 nm increased after the oxygen treatment. In particular, a significant blue shift of the absorption edge can be noticed. From the Tauc plot (inset of Figure 4), the optical energy band gap is derived to be 3.21, 3.33, and 3.37 eV for S1, S2, and S3 samples, respectively. Both, the increased optical band gap, and the enhanced optical transmittance ensure that more solar light enters, and therefore, is absorbed in the perovskite active layer of PSCs for higher photocurrent generation, as shown in Figure 1. Therefore, reduction of oxygen deficiency in TiO_2 ETM is critical for an enhanced photocurrent in PSCs.

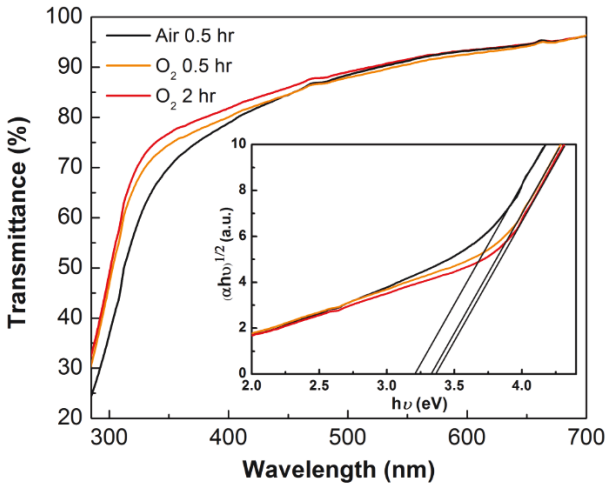

Figure 4. Transmittance of the three TiO_2 samples (S1-S3). The inset is the Tauc plots to derive their optical band gaps.

Since oxygen vacancies in TiO_2 are electron traps, density reduction of these vacancies will certainly impact the electron transport kinetics in TiO_2 ETM. To confirm this effect, the electron lifetime study and electrochemical impedance spectroscopy (EIS) measurements of PSCs were carried out. The electron lifetime, which is related to the electron recombination kinetics, was measured via the open-circuit photovoltage decay (OCVD) method.[45-49] Open circuit voltage (V_{oc}) decay was recorded in the dark condition immediately after switching off the solar illumination on PSCs, as shown in Figure 5a. Since devices were investigated under the open-circuit in the dark condition, the feature of carrier recombination could be revealed. After switching off the light, the V_{oc} of three PSCs decayed at a different rate, with PSC3 being the slowest. After 47 s, the V_{oc} decreased to 0.27, 0.39, and 0.46 V for PSC1, PSC2, and PSC3, respectively (Figure 5a). The electron recombination lifetime (τ_{er}) was calculated using the equation $\tau_{er} = -\frac{k_B T}{e}\left(\frac{\mathrm{d}V_{oc}}{\mathrm{d}t}\right)^{-1}$, where k_B is the Boltzmann constant and T is the temperature. The dependence of τ_{er} on V_{oc} is shown in Figure 5b. PSC3 exhibited a much longer electron lifetime than the other two PSCs,

especially when compared to PSC1. Since the only difference between these PSCs is the TiO_2 annealing condition, the OCVD study suggests that the oxygen treatment could reduce the density of oxygen vacancy traps in TiO_2 and further inhibit carrier recombination.

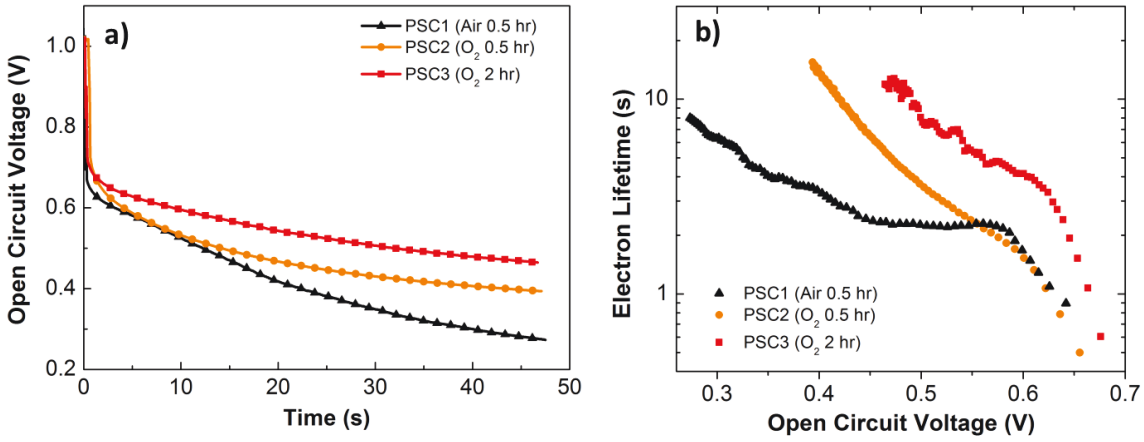

Figure 5. (a) The time transient measurement of the open circuit photovoltage after switching off the solar illumination for the three PSCs, and (b) the calculated electron recombination lifetime dependence on the open circuit voltage.

Electrochemical impedance spectroscopy (EIS) measurements of PSCs with the differently treated TiO_2 ETMs were also conducted to investigate the effect of oxygen annealing process on the charge transport kinetics and the recombination loss of PSCs. Figure 6a shows the EIS spectra of PSC1-3 in the Nyquist plot format, which exhibits two semicircle feature regions. This suggests a different carrier kinetics behavior at low and high frequencies.[50-52] It is clear that the impedance is increased from PSC1, to PSC2, and further to PSC3, indicating the dramatic effect of the TiO_2 annealing condition.

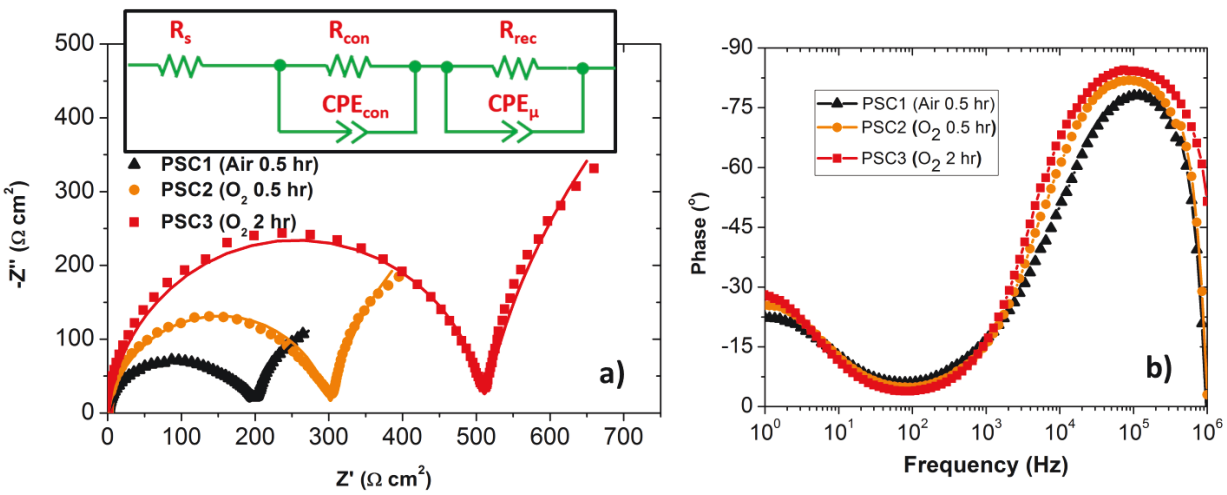

Figure 6. EIS spectra of three (PSC1, PSC2, and PSC3) cells. (a) Nyquist plots and fitting curves. Inset is the circuit used for curve fitting. (b) Bode plots showing the characteristic frequency peaks.

Table 2. Parameters extracted from EIS spectra of three PSCs.

Cell	R_s (Ω cm^2)	R_{con} (Ω cm^2)	CPE_{con} (nF cm^{-2})	p_{con}	R_{rec} (Ω cm^2)	CPE_{μ} (μF cm^{-2})	p_{μ}	f_c (kHz)	τ_{et} (μs)
PSC1 (Air 0.5 h)	1.24	191	5.87	0.82	402	3.03	0.81	120	1.32
PSC2 (O_2 0.5 h)	1.27	301	1.13	0.91	825	1.53	0.90	102	1.55
PSC3 (O_2 2 h)	1.54	508	0.24	0.95	1782	0.54	0.88	87	1.83

To extract useful information, EIS spectra were fitted using the circuit shown in the inset of Figure 6(a) consisting of two parallel-*RC* elements connected in series along with an additional series resistance (R_s). This model can describe well the measured EIS spectra, as noticed from the good fittings. In this model, the low-frequency part is attributed to the recombination resistance (R_{rec}) and chemical capacitance (CPE_{μ}) of the system, while the high-frequency semicircle is described by the contact impedance, R_{con} and CPE_{con}, between the perovskite and two selective contacts.[53] Considering the same perovskite/HTM interface being used, the difference in contact

impedance for three PSCs is due to the perovskite/TiO_2 interface.[54-56] For a better fitting, constant phase elements (*CPE* with parameter *p*) were used instead of capacitors. The fitted parameters are listed in Table 2. It is not surprising that with the reduced density of oxygen vacancies and related sub-band states in the TiO_2 ETM layer, the series resistance R_s is slightly increased, and the electron injection rate into TiO_2 is reduced, thus resulting in a slightly higher R_{con} when TiO_2 is annealed in O_2 and at longer duration. However, considering the overall PSC performance, the slightly higher contact resistance and series resistance can be offset by the concomitant increase of the recombination resistance R_{rec}, or the reduction of recombination rate of photocarriers. It is known that electrons trapped in the sub-band states of TiO_2, particularly for those close to the interface with the perovskite, will enhance recombination with holes in the perovskite. Our results clearly indicate that the reduction of density of oxygen vacancies in TiO_2 can decrease the charge recombination rate. It is interesting to note that the chemical capacitance CPE_μ is reduced after the treatment of TiO_2 in oxygen. The chemical capacitance is closely related to energy states around the electrochemical potential of the contact layer (TiO_2 here). A diminishing chemical capacitance, as measured here, again, is consistent with our observation that the oxygen treatment of TiO_2 reduces the density of oxygen vacancies and their related energy states.

With the reduction of charge traps in TiO_2, particularly those at the surface, it is expected that the charge transfer rate from perovskite into TiO_2 will decrease. To find out the electron transfer time (τ_{et}), Bode plots of EIS spectra were generated, and are shown in Figure 6b. The electron transfer time can be obtained from the characteristic frequency peaks (f_c) in the high frequency charge transfer region[57] using the relation: $\tau_{et} = (2\pi f_c)^{-1}$. It is clear from Figure 6b that the f_c value shifts towards lower frequency as the oxygenated annealing time is increased. Thus, τ_{et} is increased from 1.32 μs for PSC1 to 1.55 μs for PSC2, and 1.83 μs for PSC3. In principle, a short electron

transfer time improves PSC efficiency; however, this shortened time should not be achieved by introducing wrong electron paths such as electron deep traps since electrons transferred through such paths will not be collected at PSC electrodes. The slightly longer electron transfer time measured in PSC3 proves that the electron transfer path through deep traps have been reduced significantly comparing to PSC1. This result again confirms that the oxygen deficiency related traps were diminished after longer time annealing in oxygen.

CONCLUSION

In summary, the chemical bonding analysis and the optical emission study revealed that the oxygen vacancy related defect density in the TiO_2 electron transport layer was reduced by changing the annealing environment from ambient air to oxygen and increasing its duration. The reduced oxygen vacancy density improved the optical transmission of TiO_2 layer, and resulted in a wider optical bandgap; and therefore, the improved TiO_2 layer can serve as better optical window. More significantly, the reduction of oxygen vacancy related defects decreased the trap-assisted charge carrier recombination rate at the perovskite/TiO_2 interface, and resulted in the extended charge carrier lifetime, as confirmed by the open circuit photovoltage decay study and the electrochemical impedance spectroscopy study. This leads to an enhanced current density and an improved fill factor in the PSC; and therefore, results in a better power conversion efficiency.

ACKNOWLEDGMENTS

This work was supported by the National Science Foundation (CBET-1438681).

REFERENCES

1. Jeon, N. J.; Noh, J. H.; Yang, W. S.; Kim, Y. C.; Ryu, S.; Seo, J.; Seok, S. I. Compositional Engineering of Perovskite Materials for High-Performance Solar Cells. *Nature* **2015**, *517*, 476.
2. Zhao, Y.; Zhu, K. Solution Chemistry Engineering Toward High-Efficiency Perovskite Solar Cells. *J. Phys. Chem. Lett.* **2014**, *5*, 4175-4186.
3. Liu, X.; Zhao, W.; Cui, H.; Xie, Y. a.; Wang, Y.; Xu, T.; Huang, F. Organic–Inorganic Halide Perovskite based Solar Cells–Revolutionary Progress in Photovoltaics. *Inorg. Chem. Front.* **2015**, *2*, 315-335.
4. Liu, Z.; Zhang, M.; Xu, X.; Bu, L.; Zhang, W.; Li, W.; Zhao, Z.; Wang, M.; Cheng, Y.-B.; He, H. p-Type Mesoscopic NiO as an Active Interfacial Layer for Carbon Counter Electrode based Perovskite Solar Cells. *Dalton Trans.* **2015**, *44*, 3967-3973.
5. Mabrouk, S.; Dubey, A.; Zhang, W.; Adhikari, N.; Bahrami, B.; Hasan, M. N.; Yang, S.; Qiao, Q. Increased Efficiency for Perovskite Photovoltaics via Doping the PbI_2 Layer. *J. Phys. Chem. C* **2016**, *120*, 24577-24582.
6. Alivov, Y.; Fan, Z. Dye-Sensitized Solar Cells Using TiO_2 Nanoparticles Transformed from Nanotube Arrays. *J. Mater. Sci.* **2010**, *45*, 2902-2906.
7. O'Mahony, F. T.; Lee, Y. H.; Jellett, C.; Dmitrov, S.; Bryant, D. T.; Durrant, J. R.; O'Regan, B. C.; Graetzel, M.; Nazeeruddin, M. K.; Haque, S. A. Improved Environmental Stability of Organic Lead Trihalide Perovskite-based Photoactive-Layers in the Presence of Mesoporous TiO_2. *J. Mater. Chem. A* **2015**, *3*, 7219-7223.
8. Islam, N.; Yang, M.; Zhu, K.; Fan, Z. Mesoporous Scaffolds based on TiO_2 Nanorods and Nanoparticles for Efficient Hybrid Perovskite Solar Cells. *J. Mater. Chem. A* **2015**, *3*, 24315-24321.
9. Du, Y.; Cai, H.; Wen, H.; Wu, Y.; Huang, L.; Ni, J.; Li, J.; Zhang, J. Novel Combination of Efficient Perovskite Solar Cells with Low Temperature Processed Compact TiO_2 Layer via Anodic Oxidation. *ACS Appl. Mater. Interfaces* **2016**, *8*, 12836-12842.
10. Pathak, S. K.; Abate, A.; Ruckdeschel, P.; Roose, B.; Gödel, K. C.; Vaynzof, Y.; Santhala, A.; Watanabe, S.-I.; Hollman, D. J.; Noel, N.; Sepe, A.; Wiesner, U.; Friend, R.; Snaith, H. J.; Steiner, U. Performance and Stability Enhancement of Dye-Sensitized and Perovskite Solar Cells by Al Doping of TiO_2. *Adv. Funct. Mater.* **2014**, *24*, 6046-6055.

11. de Jongh, P. E.; Vanmaekelbergh, D. Trap-Limited Electronic Transport in Assemblies of Nanometer-Size TiO_2 Particles. *Phys. Rev. Lett.* **1996**, *77*, 3427-3430.
12. Nelson, J. Continuous-Time Random-Walk Model of Electron Transport in Nanocrystalline TiO_2 Electrodes. *Phys. Rev. B* **1999**, *59*, 15374-15380.
13. Schlichthörl, G.; Huang, S. Y.; Sprague, J.; Frank, A. J. Band Edge Movement and Recombination Kinetics in Dye-Sensitized Nanocrystalline TiO_2 Solar Cells: A Study by Intensity Modulated Photovoltage Spectroscopy. *J. Phys. Chem. B* **1997**, *101*, 8141-8155.
14. de Jongh, P. E.; Vanmaekelbergh, D. Investigation of the Electronic Transport Properties of Nanocrystalline Particulate TiO_2 Electrodes by Intensity-Modulated Photocurrent Spectroscopy. *J. Phys. Chem. B* **1997**, *101*, 2716-2722.
15. Zhang, F.; Ma, W.; Guo, H.; Zhao, Y.; Shan, X.; Jin, K.; Tian, H.; Zhao, Q.; Yu, D.; Lu, X.; Lu, G.; Meng, S. Interfacial Oxygen Vacancies as a Potential Cause of Hysteresis in Perovskite Solar Cells. *Chem. Mater.* **2016**, *28*, 802-812.
16. Zhou, H.; Chen, Q.; Li, G.; Luo, S.; Song, T.-b.; Duan, H.-S.; Hong, Z.; You, J.; Liu, Y.; Yang, Y. Interface Engineering of Highly Efficient Perovskite Solar Cells. *Science* **2014**, *345*, 542.
17. Wang, F.; Ge, W.; Shen, T.; Ye, B.; Fu, Z.; Lu, Y. The Effect of Bulk/Surface Defects Ratio Change on the Photocatalysis of TiO_2 Nanosheet Film. *Appl. Surf. Sci.* **2017**, *410*, 513-518.
18. Manseki, K.; Ikeya, T.; Tamura, A.; Ban, T.; Sugiura, T.; Yoshida, T. Mg-Doped TiO_2 Nanorods Improving Open-Circuit Voltages of Ammonium Lead Halide Perovskite Solar Cells. *RSC Adv.* **2014**, *4*, 9652-9655.
19. Yang, M.; Guo, R.; Kadel, K.; Liu, Y.; O'Shea, K.; Bone, R.; Wang, X.; He, J.; Li, W. Improved Charge Transport of Nb-Doped TiO_2 Nanorods in Methylammonium Lead Iodide Bromide Perovskite Solar Cells. *J. Mater. Chem. A* **2014**, *2*, 19616-19622.
20. Qin, P.; Domanski, A. L.; Chandiran, A. K.; Berger, R.; Butt, H.-J.; Dar, M. I.; Moehl, T.; Tetreault, N.; Gao, P.; Ahmad, S. Yttrium-Substituted Nanocrystalline TiO_2 Photoanodes for Perovskite based Heterojunction Solar Cells. *Nanoscale* **2014**, *6*, 1508-1514.
21. Zhang, X.; Bao, Z.; Tao, X.; Sun, H.; Chen, W.; Zhou, X. Sn-Doped TiO_2 Nanorod Arrays and Application in Perovskite Solar Cells. *RSC Adv.* **2014**, *4*, 64001-64005.
22. Gu, X.; Wang, Y.; Zhang, T.; Liu, D.; Zhang, R.; Zhang, P.; Wu, J.; Chen, Z. D.; Li, S. Enhanced Electronic Transport in Fe^{3+}-doped TiO_2 for High Efficiency Perovskite Solar Cells. *Journal of Materials Chemistry C* **2017**. in press, DOI:10.1039/C7TC03845C.

23. Zhang, X.; Wu, Y.; Huang, Y.; Zhou, Z.; Shen, S. Reduction of Oxygen Vacancy and Enhanced Efficiency of Perovskite Solar Cell by Doping Fluorine into TiO_2. *J. Alloys Compd.* **2016**, *681*, 191-196.
24. Choi, J.; Song, S.; Hörantner, M. T.; Snaith, H. J.; Park, T. Well-Defined Nanostructured, Single-Crystalline TiO_2 Electron Transport Layer for Efficient Planar Perovskite Solar Cells. *ACS Nano* **2016**, *10*, 6029-6036.
25. Du, Y.; Cai, H.; Wu, Y.; Xing, Z.; Li, Z.; Xu, J.; Huang, L.; Ni, J.; Li, J.; Zhang, J. Enhanced Planar Perovskite Solar Cells with Efficiency Exceeding 16% via Reducing the Oxygen Vacancy Defect State in Titanium Oxide Electrode. *Phys. Chem. Chem. Phys.* **2017**, *19*, 13679-13686.
26. Ha, S.-J.; Heo, J. H.; Im, S. H.; Moon, J. H. Mesoscopic $CH_3NH_3PbI_3$ Perovskite Solar Cells using TiO_2 Inverse Opal Electron-conducting Scaffolds. *J. Mater. Chem. A* **2017**, *5*, 1972-1977.
27. Kim, Y.; Yoo, B. J.; Vittal, R.; Lee, Y.; Park, N.-G.; Kim, K.-J. Low-Temperature Oxygen Plasma Treatment of TiO_2 Film for Enhanced Performance of Dye-Sensitized Solar Cells. *J. Power Sources* **2008**, *175*, 914-919.
28. Rajmohan, G. D.; Dai, X. J.; Tsuzuki, T.; Lamb, P. R.; du Plessis, J.; Huang, F.; Cheng, Y.-B. Modifying TiO_2 Surface Architecture by Oxygen Plasma to Increase Dye Sensitized Solar Cell Efficiency. *Thin Solid Films* **2013**, *545*, 521-526.
29. Wojciechowski, K.; Stranks, S. D.; Abate, A.; Sadoughi, G.; Sadhanala, A.; Kopidakis, N.; Rumbles, G.; Li, C.-Z.; Friend, R. H.; Jen, A. K. Y.; Snaith, H. J. Heterojunction Modification for Highly Efficient Organic–Inorganic Perovskite Solar Cells. *ACS Nano* **2014**, *8*, 12701-12709.
30. Li, Y.; Zhao, Y.; Chen, Q.; Yang, Y.; Liu, Y.; Hong, Z.; Liu, Z.; Hsieh, Y.-T.; Meng, L.; Li, Y. Multifunctional Fullerene Derivative for Interface Engineering in Perovskite Solar Cells. *J. Am. Chem. Soc.* **2015**, *137*, 15540-15547.
31. Zhu, Z.; Ma, J.; Wang, Z.; Mu, C.; Fan, Z.; Du, L.; Bai, Y.; Fan, L.; Yan, H.; Phillips, D. L. Efficiency Enhancement of Perovskite Solar Cells through Fast Electron Extraction: the Role of Graphene Quantum Dots. *J. Am. Chem. Soc.* **2014**, *136*, 3760-3763.
32. Wang, H.-H.; Chen, Q.; Zhou, H.; Song, L.; Louis, Z. S.; Marco, N. D.; Fang, Y.; Sun, P.; Song, T.-B.; Chen, H.; Yang, Y. Improving the TiO_2 Electron Transport Layer in Perovskite

Solar Cells using Acetylacetonate-based Additives. *J. Mater. Chem. A* **2015**, *3*, 9108-9115.

33. Ke, W.; Xiao, C.; Wang, C.; Saparov, B.; Duan, H.-S.; Zhao, D.; Xiao, Z.; Schulz, P.; Harvey, S. P.; Liao, W.; Meng, W.; Yu, Y.; Cimaroli, A. J.; Jiang, C.-S.; Zhu, K.; Al-Jassim, M.; Fang, G.; Mitzi, D. B.; Yan, Y. Employing Lead Thiocyanate Additive to Reduce the Hysteresis and Boost the Fill Factor of Planar Perovskite Solar Cells. *Adv. Mater.* **2016**, *28*, 5214-5221.
34. Yang, D.; Zhou, X.; Yang, R.; Yang, Z.; Yu, W.; Wang, X.; Li, C.; Liu, S.; Chang, R. P. H. Surface Optimization to Eliminate Hysteresis for Record Efficiency Planar Perovskite Solar Cells. *Energy Environ. Sci.* **2016**, *9*, 3071-3078.
35. Wang, X.; Deng, L.-L.; Wang, L.-Y.; Dai, S.-M.; Xing, Z.; Zhan, X.-X.; Lu, X.-Z.; Xie, S.-Y.; Huang, R.-B.; Zheng, L.-S. Cerium Oxide Standing out as an Electron Transport Layer for Efficient and Stable Perovskite Solar Cells Processed at Low Temperature. *J. Mater. Chem. A* **2017**, *5*, 1706-1712.
36. Cho, A.-N.; Park, N.-G. Impact of Interfacial Layers in Perovskite Solar Cells. *ChemSusChem* **2017**. in press, DOI: 10.1002/cssc.201701095.
37. Kumar, P. M.; Badrinarayanan, S.; Sastry, M. Nanocrystalline TiO_2 Studied by Optical, FTIR and X-ray Photoelectron Spectroscopy: Correlation to Presence of Surface States. *Thin solid films* **2000**, *358*, 122-130.
38. Rumaiz, A. K.; Ali, B.; Ceylan, A.; Boggs, M.; Beebe, T.; Shah, S. I. Experimental Studies on Vacancy Induced Ferromagnetism in Undoped TiO_2. *Solid State Commun.* **2007**, *144*, 334-338.
39. Battiston, S.; Leto, A.; Minella, M.; Gerbasi, R.; Miorin, E.; Fabrizio, M.; Daolio, S.; Tondello, E.; Pezzotti, G. Cathodoluminescence Evaluation of Oxygen Vacancy Population in Nanostructured Titania Thin Films for Photocatalytic Applications. *J. Phys. Chem. A* **2010**, *114*, 5295-5298.
40. Plugaru, R.; Cremades, A.; Piqueras, J. The Effect of Annealing in Different Atmospheres on the Luminescence of Polycrystalline TiO_2. *J. Phys.: Condens. Matter* **2004**, *16*, S261-S268.
41. Zhang, W. F.; Zhang, M. S.; Yin, Z.; Chen, Q. Photoluminescence in Anatase Titanium Dioxide Nanocrystals. *Appl. Phys. B* **2000**, *70*, 261-265.
42. Hosaka, N.; Sekiya, T.; Kurita, S. Excitonic State in Anatase TiO_2 Single Crystal. *J. Lumin.* **1997**, *72*, 874-875.
43. Sekiya, T.; Kamei, S.; Kurita, S. Luminescence of Anatase TiO_2 Single Crystals Annealed in

Oxygen Atmosphere. *J. Lumin.* **2000**, *87–89*, 1140-1142.

44. Sekiya, T.; Ichimura, K.; Igarashi, M.; Kurita, S. Absorption Spectra of Anatase TiO_2 Single Crystals Heat-Treated under Oxygen Atmosphere. *J. Phys. Chem. Solids* **2000**, *61*, 1237-1242.
45. Baumann, A.; Tvingstedt, K.; Heiber, M. C.; Väth, S.; Momblona, C.; Bolink, H. J.; Dyakonov, V. Persistent Photovoltage in Methylammonium Lead Iodide Perovskite Solar Cells. *APL Mater.* **2014**, *2*, 081501.
46. Bisquert, J.; Zaban, A.; Greenshtein, M.; Mora-Seró, I. Determination of Rate Constants for Charge Transfer and the Distribution of Semiconductor and Electrolyte Electronic Energy Levels in Dye-Sensitized Solar Cells by Open-Circuit Photovoltage Decay Method. *J. Am. Chem. Soc.* **2004**, *126*, 13550-13559.
47. Sun, X.; Liu, Y.; Tai, Q.; Chen, B.; Peng, T.; Huang, N.; Xu, S.; Peng, T.; Zhao, X.-Z. High Efficiency Dye-Sensitized Solar Cells based on a Bi-Layered Photoanode Made of TiO_2 Nanocrystallites and Microspheres with High Thermal Stability. *J. Phys. Chem. C* **2012**, *116*, 11859-11866.
48. Tao, H.; Fang, G.-j.; Ke, W.-j.; Zeng, W.; Wang, J. In-situ Synthesis of TiO_2 Network Nanoporous Structure on Ti Wire Substrate and its Application in Fiber Dye Sensitized Solar Cells. *J. Power Sources* **2014**, *245*, 59-65.
49. Su, T.; Yang, Y.; Dong, G.; Ye, T.; Jiang, Y.; Fan, R. Improved Photovoltaic Performance of Mesoporous Perovskite Solar Cells with Hydrogenated TiO_2: Prolonged Photoelectron Lifetime and High Separation Efficiency of Photoinduced Charge. *RSC Adv.* **2016**, *6*, 65125-65135.
50. Song, J.; Li, S.; Zhao, Y.; Yuan, J.; Zhu, Y.; Fang, Y.; Zhu, L.; Gu, X.; Qiang, Y. Performance Enhancement of Perovskite Solar Cells by Doping TiO_2 Blocking Layer with Group VB Elements. *J. Alloys Compd.* **2017**, *694*, 1232-1238.
51. Hoque, M. N. F.; Yang, M.; Li, Z.; Islam, N.; Pan, X.; Zhu, K.; Fan, Z. Polarization and Dielectric Study of Methylammonium Lead Iodide Thin Film to Reveal its Nonferroelectric Nature under Solar Cell Operating Conditions. *ACS Energy Lett.* **2016**, *1*, 142-149.
52. Hoque, M. N. F.; Islam, N.; Li, Z.; Ren, G.; Zhu, K.; Fan, Z. Ionic and Optical Properties of Methylammonium Lead Iodide Perovskite across the Tetragonal–Cubic Structural Phase Transition. *ChemSusChem* **2016**, *9*, 2692-2698.
53. Wu, R.; Yang, J.; Xiong, J.; Liu, P.; Zhou, C.; Huang, H.; Gao, Y.; Yang, B. Efficient Electron-

Blocking Layer-Free Planar Heterojunction Perovskite Solar Cells with a High Open-Circuit Voltage. *Org. Electron.* **2015**, *26*, 265-272.

54. Christians, J. A.; Fung, R. C.; Kamat, P. V. An Inorganic Hole Conductor for Organo-Lead Halide Perovskite Solar Cells. Improved Hole Conductivity with Copper Iodide. *J. Am. Chem. Soc.* **2013**, *136*, 758-764.
55. Liu, D.; Yang, J.; Kelly, T. L. Compact Layer Free Perovskite Solar Cells with 13.5% Efficiency. *J. Am. Chem. Soc.* **2014**, *136*, 17116-17122.
56. Li, J.-F.; Zhang, Z.-L.; Gao, H.-P.; Zhang, Y.; Mao, Y.-L. Effect of Solvents on the Growth of TiO_2 Nanorods and Their Perovskite Solar Cells. *J. Mater. Chem. A* **2015**, *3*, 19476-19482.
57. Chen, H.-W.; Huang, T.-Y.; Chang, T.-H.; Sanehira, Y.; Kung, C.-W.; Chu, C.-W.; Ikegami, M.; Miyasaka, T.; Ho, K.-C. Efficiency Enhancement of Hybrid Perovskite Solar Cells with MEH-PPV Hole-Transporting Layers. *Sci. Rep.* **2016**, *6*, 34319.

TOC GRAPHIC

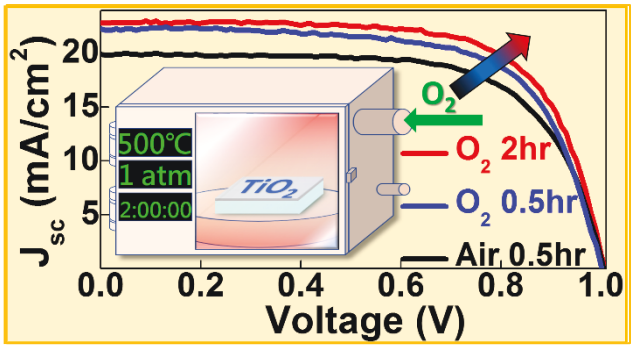
20
15
10
5
J_{sc} (mA/cm^2)
0.0
0.2
0.4
0.6
0.8
1.0
Voltage (V)
500°C
1 atm
2:00:00
TiO_2
O_2
O_2 2hr
O_2 0.5hr
Air 0.5hr